Assessing Impacts of PBL and Surface Layer Schemes in Simulating the Surface–Atmosphere Interactions and Precipitation over the Tropical Ocean Using Observations from AMIE/DYNAMO

YUN QIAN

Pacific Northwest National Laboratory, Richland, Washington

HUIPING YAN[a]

School of Atmospheric Sciences, Lanzhou University, Lanzhou, China, and Pacific Northwest National Laboratory, Richland, Washington

LARRY K. BERG, SAMSON HAGOS, AND ZHE FENG

Pacific Northwest National Laboratory, Richland, Washington

BEN YANG

School of Atmospheric Sciences, Nanjing University, Nanjing, China, and Pacific Northwest National Laboratory, Richland, Washington

MAOYI HUANG

Pacific Northwest National Laboratory, Richland, Washington

(Manuscript received 31 December 2015, in final form 20 July 2016)

ABSTRACT

Accuracy of turbulence parameterization in representing planetary boundary layer (PBL) processes and surface–atmosphere interactions in climate models is critical for predicting the initiation and development of clouds. This study 1) evaluates WRF Model–simulated spatial patterns and vertical profiles of atmospheric variables at various spatial resolutions and with different PBL, surface layer, and shallow convection schemes against measurements; 2) identifies model biases by examining the moisture tendency terms contributed by PBL and convection processes through nudging experiments; and 3) investigates the main causes of these biases by analyzing the dependence of modeled surface fluxes on PBL and surface layer schemes over the tropical ocean. The results show that PBL and surface parameterizations have surprisingly large impacts on precipitation and surface moisture fluxes over tropical oceans. All of the parameterizations tested tend to overpredict moisture in the PBL and free atmosphere and consequently result in larger moist static energy and precipitation. Moisture nudging tends to suppress the initiation of convection and reduces the excess precipitation. The reduction in precipitation bias in turn reduces the surface wind and latent heat (LH) flux biases, which suggests the positive feedback between precipitation and surface fluxes is responsible, at least in part, for the model drifts. The updated Kain–Fritsch cumulus potential (KF-CuP) shallow convection scheme tends to suppress the deep convection, consequently decreasing precipitation. The Eta Model surface layer scheme predicts more reasonable LH fluxes and LH–wind speed relationship than those for the MM5 scheme. The results help us identify sources of biases of current parameterization schemes in reproducing PBL processes, the initiation of convection, and intraseasonal variability of precipitation.

Denotes Open Access content.

[a] Current affiliations: College of Atmospheric Science, Nanjing University of Information & Technology, Nanjing, China, and and Pacific Northwest National Laboratory, Richland, Washington.

Corresponding author address: Dr. Yun Qian, Pacific Northwest National Laboratory, 902 Battelle Blvd., Richland, WA 99352. E-mail: yun.qian@pnnl.gov

DOI: 10.1175/JCLI-D-16-0040.1

© 2016 American Meteorological Society

1. Introduction

While numerical models resolve the large-scale flow, parameterizations are required for representing the effect of subgrid processes in the atmosphere such as radiation, convection, and turbulence that cannot be explicitly resolved by a numerical gridpoint model. While all physical parameterization packages play different roles in simulating the atmospheric processes, the turbulence parameterization is especially important for accurate representation of the planetary boundary layer (PBL) processes and predicting boundary layer temperature, humidity, wind, and mixed-layer depth, all of which are critical for predicting the initiation and development of convective clouds, precipitation, air quality, and land–atmosphere–cloud interactions (e.g., Cha et al. 2008; Shin and Hong 2011; Hu et al. 2010, 2013; Xie et al. 2012; Qian et al. 2013; Yang et al. 2013; Cohen et al. 2015). In addition, subgrid turbulence has a significant influence on the resolved scales owing to the complex nonlinear nature of the atmosphere; hence, it is important to parameterize vertical turbulent fluxes and subgrid-scale condensation throughout the grid column in a realistic manner (Golaz et al. 2002; Guo et al. 2014, 2015; Cheng and Xu 2015).

The importance of PBL parameterizations in weather and climate models has been extensively explored over the past several decades. For example, several studies (e.g., Hong and Pan 1996; Braun and Tao 2000; Li and Pu 2008) suggested that the skill of weather-forecasting models is sensitive to the vertical mixing formulation and that for accurate hurricane simulations, PBL schemes are as important as cloud microphysics schemes. Based on ensemble simulations from the Weather Research and Forecasting (WRF) Model using three cumulus schemes, three microphysics schemes, and two PBL schemes, Jankov et al. (2005) found that cumulus schemes had the largest effect on model performance followed by PBL schemes. Many PBL parameterizations have been developed for representing the turbulence process and its impacts in global or mesoscale models of the atmosphere (e.g., Mellor and Yamada 1974, 1982; Zhang and Anthes 1982; Stull 1984; Wyngaard and Brost 1984; Troen and Mahrt 1986; Janjić 1990; Pleim and Chang 1992; Shafran et al. 2000). Meanwhile, many studies have compared the impacts of different PBL schemes on PBL characteristics and model performance (e.g., Mahfouf et al. 1987; Pan et al. 1994; Braun and Tao 2000; Bright and Mullen 2002; Berg and Zhong 2005; Shin and Hong 2011; Hu et al. 2010, 2013; Huang et al. 2013; Xie et al. 2012). However, these studies have generally focused on evaluations against measurements collected over a single terrestrial location and turbulence regime over land, with only limited studies dedicated to comparisons between predicted and observed turbulence statistics [e.g., the surface sensible heat (SH) and latent heat (LH) fluxes; Betts et al. 1997], and rigorous evaluations of the performance of different suites of surface layer, PBL, and cumulus parameterizations are rare.

An ideal turbulence parameterization should skillfully handle different turbulence regimes and show consistent behavior over different underlying surfaces. In fact, land–atmosphere–cloud interactions are constrained not only by the surface energy balance but also by the moisture availability at the land surface, where it is challenging to sort out the relative roles of surface energy and water budgets on the thermodynamic state of the PBL and potentially the initiation of clouds. In contrast, moisture is always abundant over the ocean surface, making this an idealized regime for identifying key factors that influence the surface–atmosphere interaction and quantifying their impacts on the PBL structure given unlimited moisture supply. Therefore, it is of scientific interest to investigate the performance of different PBL, surface layer (SL), and shallow convection (SC) schemes over an oceanic surface.

The WRF Model embeds multiple parameterization options for many subgrid processes, including suites of different PBL, convection, and SL schemes (Skamarock et al. 2008). In convective environments it is important to study the combined suite of parameterizations because each plays a role in the initiation of convective clouds. The sensitivity of the model results to SL and SC parameterizations, both of which are tightly linked to the PBL parameterization, is also investigated to assess the relative contributions of these parameterizations to typical features of each PBL scheme. The observations collected during the 2011 Atmospheric Radiation Measurement Program (ARM) Madden–Julian oscillation (MJO) Investigation Experiment (AMIE)/Dynamics of the MJO (DYNAMO) field campaign (Yoneyama et al. 2013) over the Indian Ocean are used as benchmarks for assessing model performance.

Our goal is to test a subset of the various parameterizations that are available in the WRF Model and to identify the sources of bias and errors in current PBL, SL, and SC schemes, including errors related to the initiation of convection and intraseasonal variability of precipitation, with the ultimate goal of developing improved parameterizations. In this study, we have attempted to address our goal in three ways: 1) evaluate and compare the modeled spatial patterns of precipitation and surface fluxes as well as vertical profiles of potential temperature, humidity, moist static energy (MSE), and moisture tendency terms using different horizontal resolutions, PBL, SL, and SC schemes; 2) identify model biases by analyzing moisture tendency terms contributed by PBL and convection processes through a series of nudging experiments; and 3) evaluate the dependence of modeled surface latent heat fluxes to different PBL and SL schemes over the tropical ocean.

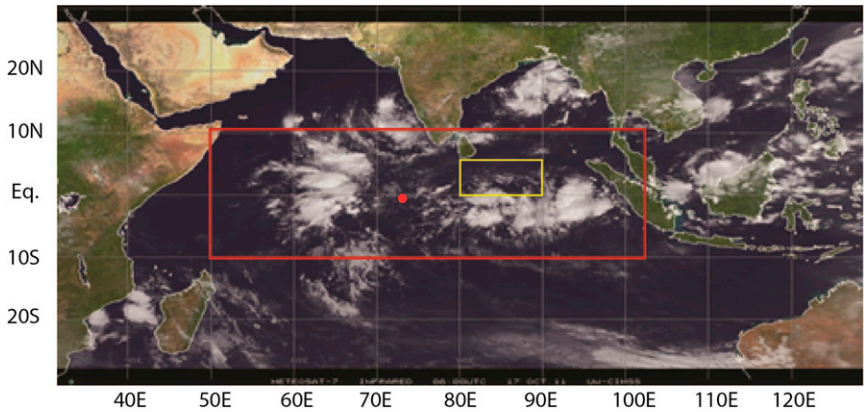

FIG. 1. Model domain and measurement network. The model domain is marked by the red rectangle and covers 11°S–11°N and 50°–102°E of the tropical Indian Ocean. Addu Atoll (0.6°S, 73.1°E), Gan Island, and the Maldives, where surface and sounding data are collected, are marked by a red dot. R/V *Roger Revelle* shipborne measurement areas are highlighted by a yellow rectangle. For more details on ship tracks, see Fig. 10.

The WRF regional climate model—including the PBL, SL, and SC schemes as well as simulation setup—and observational datasets are described in section 2. Section 3 presents the model evaluation against the observations and the details of the impact of PBL, SL, and SC schemes on the surface fluxes, cloud development, and precipitation cycle. The diagnosis of the causes of model biases that are identified are also presented in section 3. Conclusions and discussion are provided in section 4.

2. Model and observations

a. WRF Model

The Advanced Research version of WRF, version 3.4 (Skamarock et al. 2008), is used in this study. WRF is a fully compressible and nonhydrostatic model that uses a terrain-following hydrostatic-pressure vertical coordinate and an Arakawa C-grid staggering spatial discretization for variables. The simulation domain covers 11°S–11°N and 50°–102°E of the tropical Indian Ocean (Fig. 1) with two horizontal grid spacings: 10 and 50 km, with 27 sigma levels (with 4–6 levels in PBL) from the surface to 10 hPa. Wind, temperature, water vapor, pressure, and underlying surface variables including sea surface temperature used to generate initial and boundary conditions are derived from the National Centers for Environmental Prediction (NCEP) final analysis (FNL) 1° × 1° global data with 6-hourly time intervals. All simulations start on 15 October and end on 1 December 2011, and our analysis focuses on November 2011.

To investigate the impact of PBL, SL, and SC parameterizations on the simulation of tropical convection, a series of free-running simulations were completed using 10- and 50-km horizontal grid spacing. In each case, we conducted simulations using three PBL schemes: Yonsei University (YSU; Hong et al. 2006; Sterk et al. 2013), Mellor–Yamada–Janjić (MYJ; Janjić 1994), and University of Washington (UW; Bretherton and Park 2009). In this study, we have utilized the Kain–Fritsch (KF; Kain and Fritsch 1993; Kain 2004) convective scheme. To quantify the relevant tendency and model bias in water vapor, we conducted a second series of simulations using 50-km resolution, where the water vapor was nudged to values derived from the NCEP–NCAR reanalysis with a nudging time scale of 12 h at all levels. Because the YSU scheme only utilizes the MM5 Monin–Obukhov similarity SL scheme and the MYJ PBL scheme only adopts the Eta Model SL scheme, respectively, we conducted simulations using the UW PBL scheme with both MM5 and Eta Model SL schemes to compare with the YSU and MYJ simulations, respectively. The KF cumulus potential (KF-CuP) convective scheme is a version of the KF scheme modified by Berg et al. (2013) to better account for shallow clouds, which is used to compare with the standard KF to study the impact of different convection schemes on tropical convections. The Rapid Radiative Transfer Model for GCMs (RRTMG) scheme (Barker et al. 2003; Pincus et al. 2003), the WRF single-moment 6-class microphysics scheme (WSM6; Hong and Lim 2006), and the Noah land surface model (LSM; Chen and Dudhia 2001; Ek et al. 2003) are used in all simulations except for the MYJ–CuP–Eta simulation, which is currently only coupled with the Community Atmosphere Model (CAM) shortwave radiation scheme (CAM3.0; Collins et al. 2004). A quick check suggests that the impacts of the different radiation schemes used in the

TABLE 1. Experiments and corresponding SC, PBL, and SL schemes selected in this study.

Expt	Grid spacing (km)	SC scheme	PBL scheme	SL scheme	Nudging	Radiation scheme
MYJ–KF–Eta	10 and 50	KF	MYJ	Eta Model	On and off	RRTMG
UW–KF–Eta	10 and 50	KF	UW	Eta Model	On and off	RRTMG
UW–KF–MM5	10 and 50	KF	UW	MM5	On and off	RRTMG
YSU–KF–MM5	10 and 50	KF	YSU	MM5	On and off	RRTMG
MYJ–CuP–Eta	10 and 50	KF-CuP	MYJ	Eta Model	On and off	CAM

MYJ–CuP–Eta simulation on results presented in this study are minor.

b. PBL schemes

PBL schemes are used to parameterize the unresolved turbulent vertical fluxes of heat, momentum, and constituents such as water vapor or pollutants within the planetary boundary layer. Of the three PBL schemes tested in this study (Table 1), the MYJ and UW schemes apply a local turbulence kinetic energy (TKE)-based closure, while one, the YSU scheme, is a first-order nonlocal closure model. Generally, a local scheme only accounts for gradients within adjacent vertical levels in the model, but a nonlocal scheme accounts for vertical transport over a deeper layer spanning multiple levels to better represent mixing associated with thermals in the convective PBL. The MYJ scheme determines the eddy diffusivity from a prognostic treatment of TKE with local vertical mixing (Mellor and Yamada 1982).

The YSU scheme is a first-order nonlocal model, with a countergradient term in the eddy-diffusion equation designed to account for surface-driven nonlocal mixing spanning the whole boundary layer and with an explicit entrainment flux term to account for entrainment at the top of the convective PBL (Hong et al. 2006). The YSU scheme is modified for WRF, version 3.4, by Hong et al. (2006) by increasing the critical bulk Richardson number from 0 to 0.25 over land, thereby enhancing mixing in the stable boundary layer (Hong and Kim 2008). The YSU scheme has been widely used in WRF in meteorological and atmospheric chemistry studies (Hong and Kim 2008; Shin and Hong 2011). It generally captures the vertical structure of meteorological and chemical variables during unstable conditions (Storm et al. 2009; Hu et al. 2012), and the change of bulk Richardson number is likely of little consequence in the context of this study that is focused on conditions over the tropical ocean where very few periods with stable conditions are identified.

The UW moist turbulence scheme, which combines a 1.5-order turbulent closure model with an entrainment closure at the boundary layer top (Grenier and Bretherton 2001), was originally designed to improve the simulation of stratocumulus clouds. The parameterization has been modified to improve its numerical stability and performance with long time steps typically used in climate models. In contrast to the MYJ scheme, the UW scheme uses TKE as a diagnostic rather than a prognostic variable. The UW scheme also features components such as the use of moist-conserved variables, explicit entrainment closure for convective layers, improved formulation of TKE transport as a relaxation to layer-mean TKE that is efficient with longer model time steps, and unified treatment of all turbulent layers in each atmospheric column (Bretherton and Park 2009).

c. Surface layer schemes

Within WRF, surface schemes represent the effects of underlying surface, for example, calculating surface sensible and latent heat fluxes. More specifically, the SL schemes compute friction velocity u_* and other exchange coefficients that provide the basis to estimate surface heat and moisture fluxes in the land surface model and surface stress in the PBL scheme. Over water surfaces, including that of ocean in this study, the surface fluxes and other diagnostic fields are calculated in the SL parameterizations themselves.

In this study, we tested two SL schemes—the MM5 (Zhang and Anthes 1982; Beljaars 1995) and Eta Model SL schemes (Janjić 1994). Both schemes use Monin–Obukhov similarity theory (Monin and Obukhov 1954) and standard similarity functions. While the MM5 SL scheme is based on Monin–Obukhov theory with a Carlson–Boland viscous sublayer, the Eta Model scheme, developed first in the Eta Model, is based on Monin–Obukhov theory with Zilitinkevich thermal roughness length. It should be noted that only a limited number of combinations of PBL and SL schemes can be used in the community version of WRF. The YSU PBL scheme can only be used with the MM5-similarity SL scheme. The MYJ PBL scheme can only be run with the Eta Model–similarity SL scheme. The UW PBL scheme can work with both MM5-similarity and Eta Model–similarity SL schemes. It is appropriate to compare the impact of SL schemes when the same PBL scheme is applied.

d. Shallow convection scheme

All of the simulations make use of the KF cumulus parameterization (Kain and Fritsch 1993; Kain 2004). While the parameterization is designed to account for shallow cumulus, in practice they are significantly

underpredicted. To address this concern, Berg et al. (2013) developed modified version of the KF scheme, the KF-CuP scheme. To better account for the presence of shallow clouds, they replaced the ad hoc trigger function being used in the default KF scheme with a trigger function related to the PDF of temperature and humidity in the convective boundary layer (Berg and Stull 2004, 2005). To implement CuP, a number of additional modifications have been made to the standard version of KF scheme in WRF (e.g., changing the trigger function and changing the methodology used for the computation for the cloud fraction based on the time scales relevant for shallow cumuli). These changes account for subgrid variability within the convective boundary layer in a more realistic way than is done in the default application of the KF scheme. The results presented by Berg et al. (2013) show that the KF-CuP parameterization does a much better job simulating the cloud onset time, and cloud macrophysical properties (such as cloud fraction and cloud-base height) of shallow cumulus for a continental location than was possible using the standard KF parameterization.

e. Observations

The observational data used in this study are from the AMIE/DYNAMO field campaign (Yoneyama et al. 2013). The ground-based radar rainfall estimates, atmospheric sounding data from Addu Atoll (0.6°S, 73.1°E) in the Maldives, and R/V *Roger Revelle* shipborne near-surface observations are used in this study. Their locations are highlighted in Fig. 1. The National Center for Atmospheric Research (NCAR) S-band (10-cm wavelength) dual-polarization Doppler radar (S-Pol) was deployed on the atoll from 1 October 2011 to 15 January 2012 during AMIE/DYNAMO. S-Pol has a 0.9° beamwidth with a maximum range of 150 km. During AMIE/DYNAMO, S-Pol was operated on a 15-min cycle that included 360° azimuthal plan position indicator (PPI) scans. A total of eight elevation angles from 0.5° to 11° were performed for the PPI scans, and data were recorded in 1° azimuthal resolution. More details about the operating status and rainfall characteristics observed by S-Pol during AMIE/DYNAMO are provided by Zuluaga and Houze (2013) and Rowe and Houze (2014).

The S-Pol data are gridded to a Cartesian grid with a horizontal resolution of 2 km and a vertical resolution of 0.5 km using the NCAR Radx package (Mohr and Vaughan 1979). S-Pol rainfall estimates from 1 to 30 November 2011 are used in this study to validate the WRF-simulated rainfall. The rainfall estimate is produced using the "hybrid algorithm" (Ryzhkov et al. 2005), which is a combination of a simple reflectivity and rainfall rate (Z–R) relationship and several more advanced polarimetric parameter–based methods (for more details see the S-Pol rain-rate computation documentation; http://www.eol.ucar.edu/projects/dynamo/spol/parameters/rain_rate/rain_rates.html). The gridded S-Pol rain rate at 2.5-km height out to 150-km radius is averaged for each 15-min scan and further averaged to each hour to obtain the hourly domain mean rain rate. To compare with the model-simulated rainfall at the surface, the S-Pol hourly domain mean rain rate at 2.5-km height is converted to 0.5-km height using the linear function provided by Hagos et al. (2014, see their appendix A). The linear function is derived by comparing the S-Pol domain mean convective and stratiform rain rates between 2.5 and 0.5 km in height, respectively. Only the total rain rate at 0.5 km (sum of convective and stratiform rain) is used in this study. Although verification of the AMIE/DYNAMO radar-based rainfall product is an active research effort, a recent study by Thompson et al. (2015) reported that the current Z–R relationship used in the released version of the S-Pol rainfall data product could have a bias of ~10%. We used the released version of the S-Pol rainfall product available to us at the time of this study and acknowledged that future improvement and uncertainty reduction is possible.

The sounding data used in this study are from the Atmospheric Radiation Measurement Program interpolated sonde value-added product (Troyan 2012) at the Addu Atoll (Gan Island). The product uses a combination of observations from radiosondes (8 day^{-1} during AMIE/DYNAMO), surface meteorology, and microwave radiometer with a sophisticated scaling and interpolation scheme applied to the water vapor mixing ratio to produce accurate profiles of the atmospheric thermodynamic state at 1-min temporal resolution and a total of 316 altitude levels.

Near-surface meteorology measurements made on the R/V *Roger Revelle*, stationed around the equator near 80°E during AMIE/DYNAMO, are also used in this study. Details of the measurements and associated measurement systems can be found in de Szoeke et al. (2015). Wind speed, temperature, and humidity measurements were made from the bow of the ship at heights ranging from approximately 15 to 20 m above the ocean surface. The bulk fluxes of sensible and latent heat used in this study were derived using the COARE, version 3.0, algorithm (Fairall et al. 1996, 2003) for 10-min time periods and are a standard AMIE/DYNAMO data product.

Three different monthly precipitation datasets are also used for model evaluations, including 1) the Global Precipitation Climatology Project (GPCP) dataset

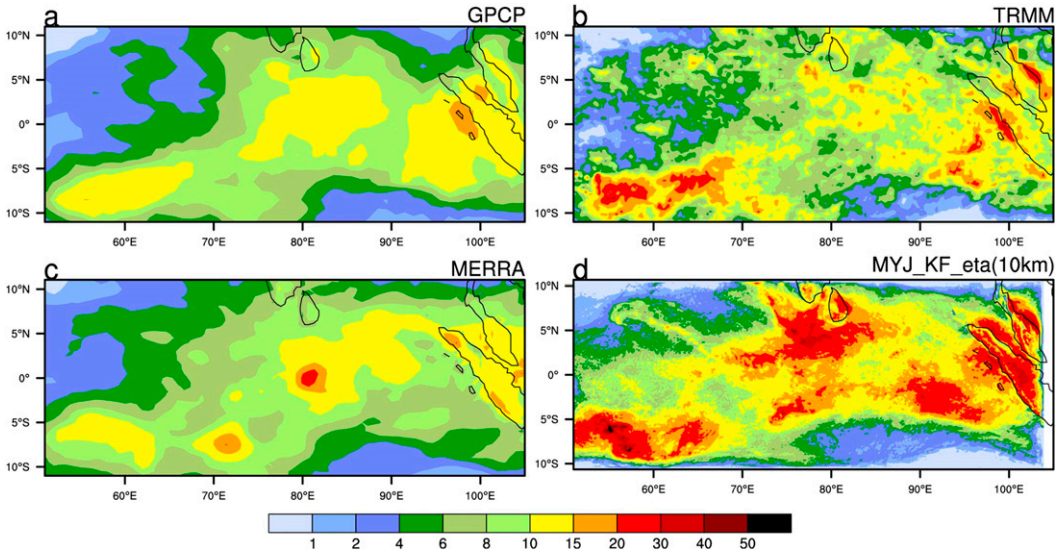

FIG. 2. Monthly mean precipitation (mm day^{-1}) in November 2011 for the simulation at 10-km spatial resolution with the MYJ PBL and Eta Model SL schemes and three sets of corresponded observations (GPCP, TRMM, and MERRA).

(Huffman et al. 1997; Adler et al. 2003); 2) the Tropical Rainfall Measuring Mission (TRMM; Kummerow et al. 1998) precipitation dataset; and 3) the Modern-Era Retrospective Analysis for Research and Applications (MERRA) dataset, which was conducted by the National Aeronautics and Space Administration (NASA) Goddard Space Flight Center (GSFC; Bosilovich 2008).

3. Results

a. Evaluation and comparison of precipitation

While the focus of this work is to quantify biases and identify the weakness of current PBL, SL, and SC schemes, an overview of the observed and modeled mean precipitation is presented first. Figure 2 shows the monthly mean precipitation in November 2011 from the three sets of observations and the simulations completed using the MYJ PBL and Eta Model SL schemes at 10-km spatial resolution. The domain-average mean (maximum) precipitation rates are 8.27 (35.08), 7.21 (20.59), 7.46 (23.90), and 10.81 (64.44) mm day^{-1} for the TRMM, GPCP, MERRA, and WRF 10-km simulations, respectively. Maximum precipitation rates of larger than 10 mm day^{-1} can be seen over the sea in the vicinity of the Mascarene Islands and the northeastern portion of the Indian Ocean as well as Sumatra and Malaysia. In general, the spatial pattern of precipitation is consistent among the three observations, except that TRMM provides larger spatial variability and values of maximum rainfall, likely owing in part to its higher spatial resolution. The Indian Ocean dipole/zonal mode, which develops in boreal summer and peaks in boreal fall when the Pacific sea surface temperature (SST) anomalies are large, together with the remote influence of El Niño–Southern Oscillation (ENSO), contributes significantly to rainfall and wind variability over the tropical Indian Ocean in fall (Webster et al. 1999). During the 2011 AMIE/DYNAMO field campaign, the eastward propagation of an MJO episode observed in late November contributes to the maximum precipitation in the northeastern Indian Ocean. In contrast, the maximum precipitation in the southwestern portion of the ocean is mainly contributed by convection associated with the ITCZ. All simulations predict too much and too frequent large amounts of precipitation (greater than 22 mm day^{-1}) but too little light and moderate precipitation (less than 20 mm day^{-1}) over the tropical ocean. Among all our simulations the configuration with the KF-CuP and Eta Model schemes best predicts the precipitation PDF against the observations. The simulated monthly precipitation clearly has a spatial pattern similar to the observations in some key regards. The model approximately captures the locations of maximum rainfall, although the 10-km simulations overpredict precipitation over a majority of the domain. The mechanisms responsible for the overprediction will be discussed in section 3c.

The free-running simulations for November 2011 all overpredict the precipitation over the model domain (Fig. 3). The simulations using the MYJ PBL parameterization are in the best agreement with the observations and the mean bias is smaller than 1 mm day^{-1}, with the run with KF-CuP being better than the run

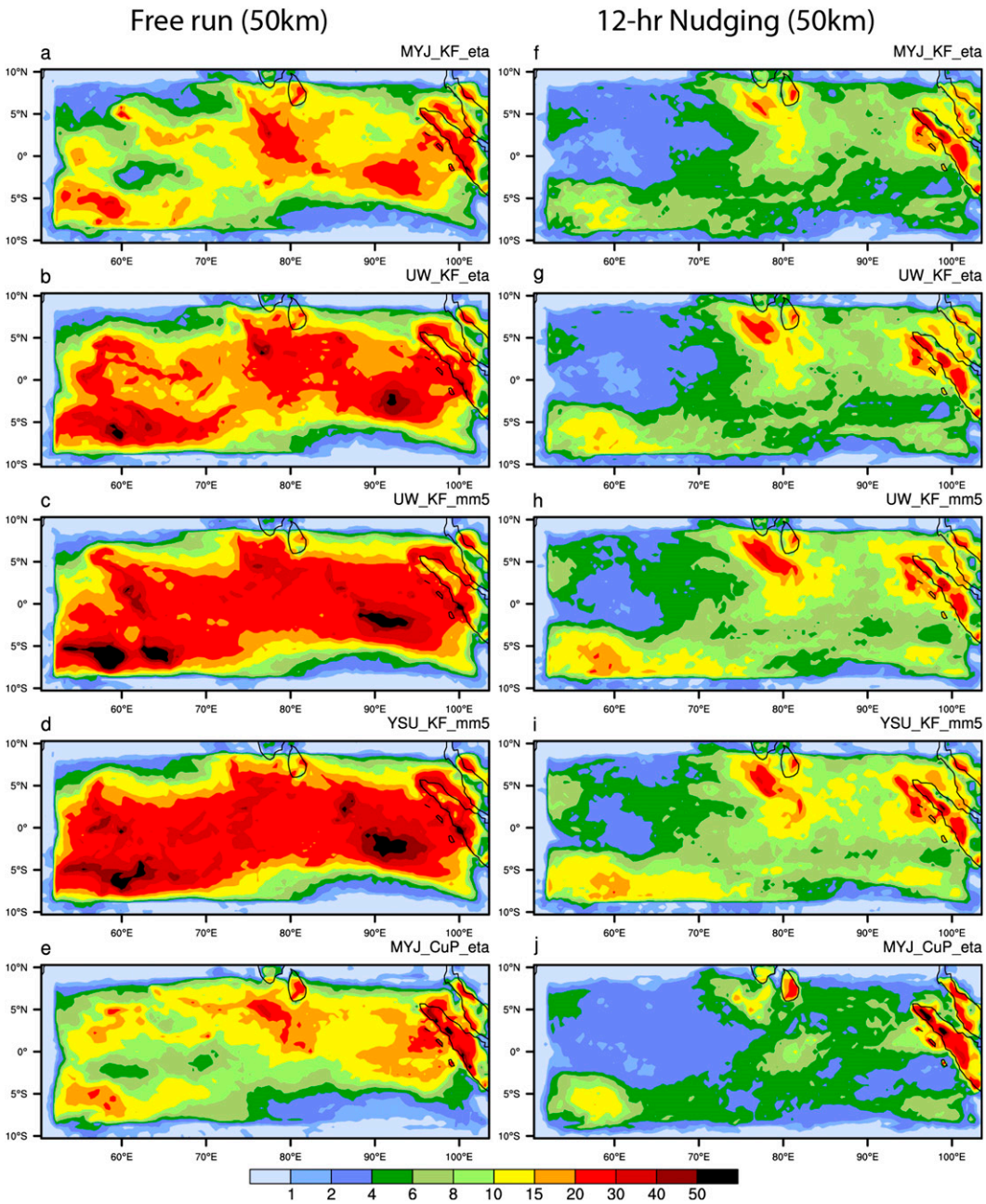

FIG. 3. Monthly mean precipitation (mm day^{-1}) in November 2011 for the simulation at 50-km spatial resolutions in (a)–(e) free-running and (f)–(j) moisture-nudged experiments with different schemes as shown in Table 1.

with the standard KF parameterization (Figs. 3a,e and Table 2). The run with the UW PBL parameterization coupled with the Eta Model SL parameterization simulates more precipitation (with mean bias of 4.78 mm day^{-1}) than is found for the run with the MYJ PBL parameterization (Figs. 3a,b). The UW PBL scheme can be run with both the Eta Model and MM5 SL schemes, enabling investigation of the sensitivity to the SL parameterization (Figs. 3b,c). The simulation utilizing the MM5 SL parameterization has much larger amounts of precipitation (with mean biases of 7.59 mm day^{-1} for UW–KF–MM5 and 8.21 mm day^{-1} for YSU–KF–MM5) than is the case for the simulations with the Eta Model SL parameterization. The systematic differences in the behavior of the SL parameterization will be explored further in section 3d. The only nonlocal PBL parameterization used in the study simulates the largest amounts of precipitation and could be

TABLE 2. Statistics of model evaluation against TRMM. All simulations use 50-km horizontal resolution except for MYJ–KF–Eta-10, which uses 10-km resolution. The numbers in parentheses are for corresponding nudging simulations (see Fig. 3).

Expt	Mean bias (mm day^{-1})	RMSE	Pattern correlation
MYJ–KF–Eta	0.84 (−2.88)	6.47 (5.29)	0.82 (0.84)
UW–KF–Eta	4.78 (−2.42)	10.83 (5.17)	0.80 (0.84)
UW–KF–MM5	7.59 (−1.43)	14.34 (5.07)	0.79 (0.85)
YSU–KF–MM5	8.21 (−1.25)	15.09 (5.04)	0.78 (0.85)
MYJ–CuP–Eta	0.31 (−3.83)	6.71 (6.62)	0.80 (0.71)
MYJ–KF–Eta-10	2.52	6.83	0.87

related to an overestimate in the vertical transport of water vapor or a boundary layer that is too deep.

When nudging is applied, all of the model configurations except for MYJ–CuP–Eta do a much better job simulating the observed precipitation than the free-running simulations. The mean bias and root-mean-square error associated with the nudged simulations are much smaller, and the spatial pattern correlation is higher than that in free-running simulations (see Table 2). The motivation for using nudging in this application is to help us diagnose sources of model biases rather than to obtain a best model configuration for precipitation simulations. Specifically, comparisons of the tendencies associated with the nudging can be compared with the tendencies with those from the WRF parameterizations to help identify processes that are not accurately represented in the free-running simulations [see Hagos et al. (2011) for an example of the strategy]. This point will be further discussed in section 3c.

An analysis of the time series of daily precipitation observed over the Addu Atoll and from a subset of the simulations highlights the systemic bias in the precipitation (Fig. 4). In this case the free-running and nudged simulations were run using the YSU PBL and MM5 SL parameterizations. Model results with nudging show that both the timing and magnitude of simulated precipitation are greatly improved (please note a few erroneous precipitation episodes in the free-running simulations in the first few days of the month have been removed in the nudged simulations).

b. *Vertical profiles*

To further investigate thermodynamic impacts of PBL and SL schemes on convective clouds and precipitation, vertical profiles of several key thermodynamic parameters have been created using both observations from the ARM radiosondes and model results averaged over November 2011 over the Maldives (Fig. 5). The overall structure of the profiles is similar for both observation and simulations, especially for potential temperature, with the top of the well-mixed boundary layer located at approximately 0.5 km above sea level, with relatively good

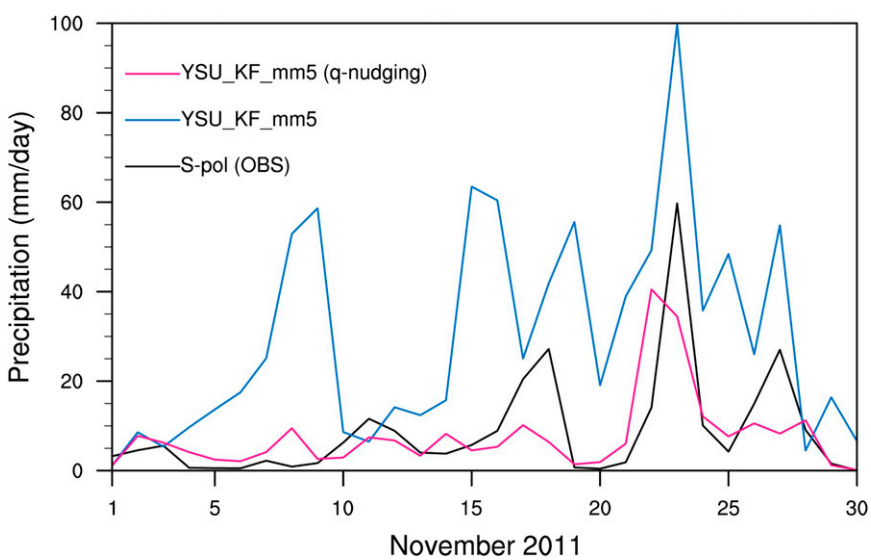

FIG. 4. Time series of precipitation in November 2011 from S-Pol measurement over the Gan site and free-running and moisture-nudged simulations with the YSU–KF–MM5 scheme.

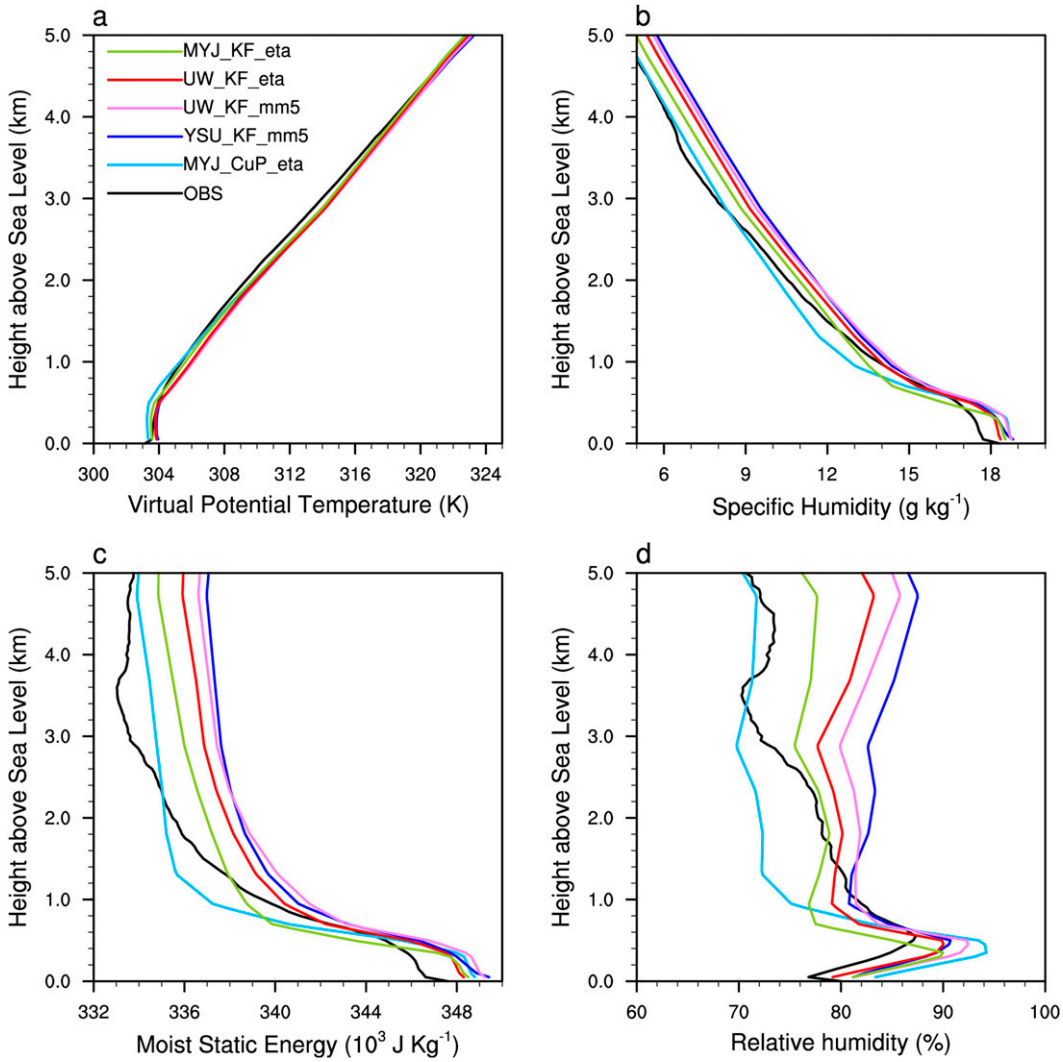

FIG. 5. Vertical profiles of virtual potential temperature (VPT), specific humidity, MSE, and RH averaged in November 2011 from observation over the Maldives and five free-running simulations with different PBL, SC, and SL schemes.

agreement in the simulated and observed PBL depth (Figs. 5a,b). However, noticeable systematic biases can be found in both the PBL and free troposphere for specific humidity, moist static energy, and relative humidity in all the free-running simulations.

The specific humidity is overpredicted by 8%–10% in the PBL and upper levels in the troposphere in all free-running simulations. Consistent with specific humidity, the moist static energy in all simulations is also greater than that observed within the low boundary layer and upper levels, indicative of additional convection and precipitation. The relative humidity increases with altitude from the surface and reaches a peak at the top of the boundary layer and then gradually decreases in the troposphere. The biases in specific humidity and moist static energy are consistent with the wet and warm biases in precipitation and temperature, respectively. That is, excess simulated precipitation leads to the release of latent energy that warms the troposphere, which is induced by the transport of moisture through the top of the PBL.

Overall, the SL schemes simulate much stronger evaporation (analyzed later in section 3d), bringing too much water vapor into the boundary layer. Meanwhile, PBL schemes vertically transport the overpredicted water vapor from near surface to the upper layers of the PBL, which leads to the wet bias in the free troposphere due to the vertical transport of moisture out of the PBL by shallow or deep convections. The lower troposphere over the tropical ocean is close to quasi equilibrium when averaged over a period of time. Therefore, the MSE at the base of the free troposphere is coupled to

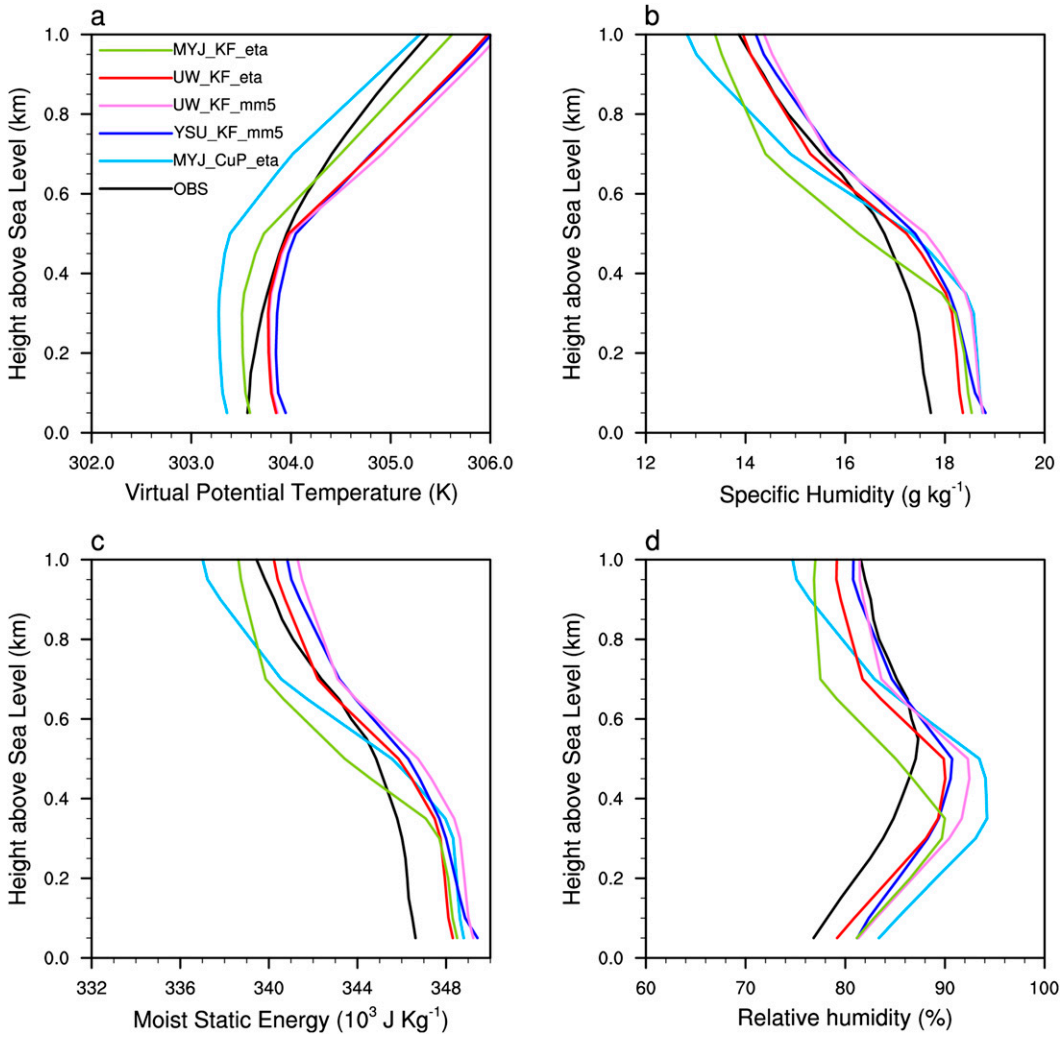

FIG. 6. As in Fig. 5, but for heights ranging from 0 to 1 km.

that at the top of the PBL. In other words, the profiles in the lower troposphere are more or less controlled by what happens within the PBL, following the work of Emanuel (2007). In simulations with the same PBL scheme (UW), the MM5 SL scheme generates larger moisture biases than that associated with the Eta Model scheme in both the PBL and free troposphere (as seen by comparing the pink and red lines in Figs. 5 and 6). In contrast, in simulations with the same SL scheme (Eta Model), the UW scheme produces smaller moisture biases than the MYJ scheme in PBL but has larger biases in upper levels most likely because of the stronger vertical mixing of air in the UW scheme that can bring more water vapor to the PBL top, favoring the initiation and development of convection (as seen by comparing the red and green lines in Figs. 5 and 6). With the same SL scheme (MM5), the UW scheme generates larger moisture bias than the YSU scheme in PBL but smaller biases in the free troposphere. This is because the nonlocal YSU scheme simulates stronger vertical mixing in unstable conditions (Shin and Hong 2011; Xie et al. 2012). With the same SL scheme (Eta Model) and PBL scheme (MYJ), the CuP scheme tends to suppress the development of deep convection and evidently reduces the wet moisture bias in the free troposphere, resulting in a large reduction in precipitation bias (Fig. 3j).

To quantify the possible impact of excessive latent heat flux on the moist bias in the simulated PBL, we also compare the vertical shape (gradient) of profiles by normalizing by their respective values at the surface to better understand the behavior of the PBL schemes under similar surface forcing. Most of the differences shown in Fig. 5 are found in the figure with the

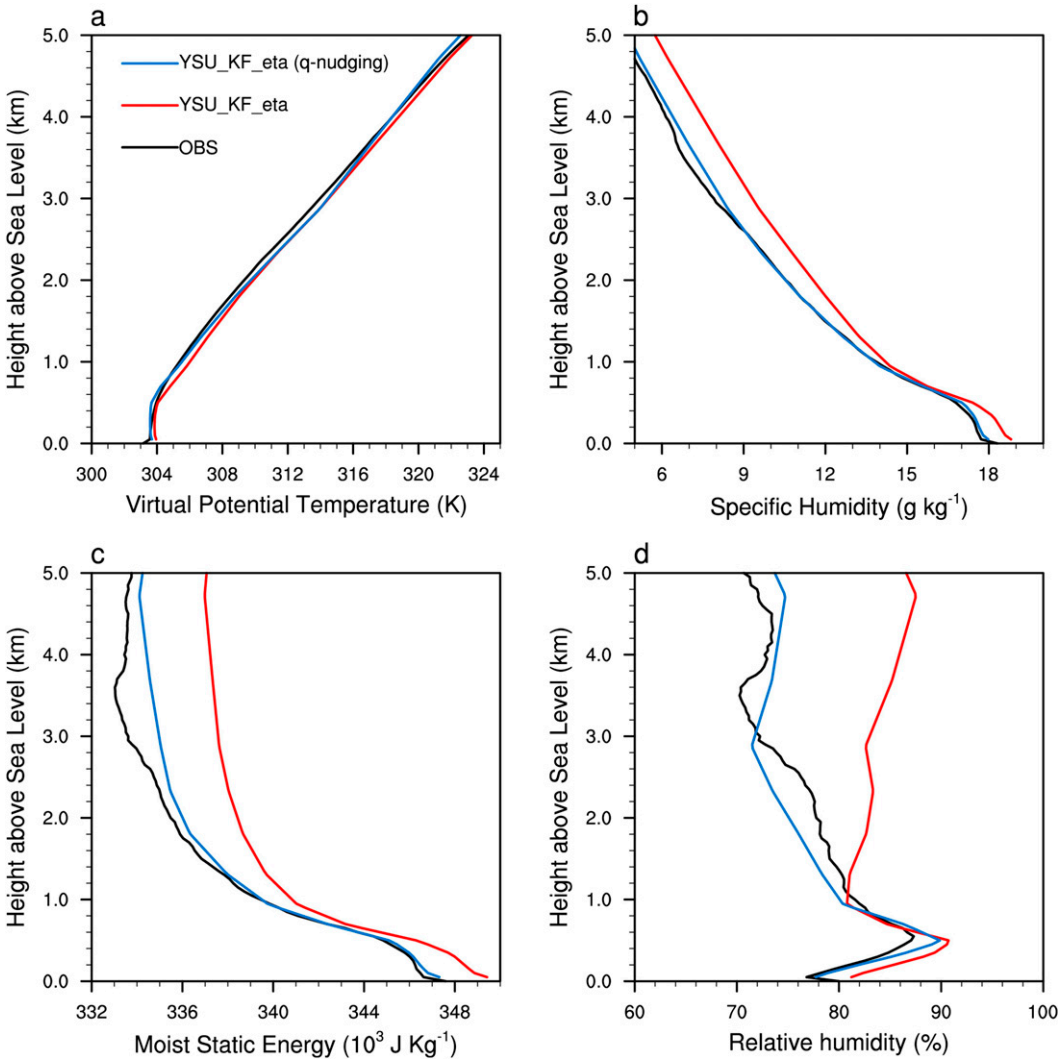

FIG. 7. As in Fig. 5, but for simulations using the YSU–KF–MM5 scheme with and without moisture nudging.

normalized profiles (not shown) as well. All the schemes mix the PBL more effectively than is observed, and they deliver more moisture and MSE to the top of the PBL. This suggests the excess moisture and precipitation bias is likely related to problems in the PBL schemes in addition to the excess fluxes from the surface schemes.

c. *Bias diagnosis based on nudging tendency analysis*

A perfect SL and PBL scheme would provide correct mean profiles and would accurately predict the variability. However, the results presented in section 3b from free-running simulations show large moisture biases among different schemes in both the PBL and free troposphere. We conduct another set of simulations with the same set of PBL, SL, and SC schemes but nudge the water vapor to NCEP FNL data (temperature and wind are not nudged), with a nudging time scale of 12 h. Using YSU with MM5 as an example, Fig. 7 shows a comparison of vertical profiles in corresponding simulations completed with or without moisture nudging. It is not surprising that the moisture nudging only slightly modifies the potential temperature profile but significantly removes the overpredicted water vapor in both the PBL and free troposphere found in the free-running simulations. In the nudged simulation, the air temperature above an altitude of 3 km is slightly lower than that in the free run, mainly resulting from the suppressed deep convection. Meanwhile, positive biases in MSE and relative humidity are also corrected in the moisture-nudging simulations. Consequently, the overprediction of precipitation in the free-running simulation, including the rainfall episode around 23 November, is dramatically reduced when moisture nudging is applied in the simulations (see Fig. 4).

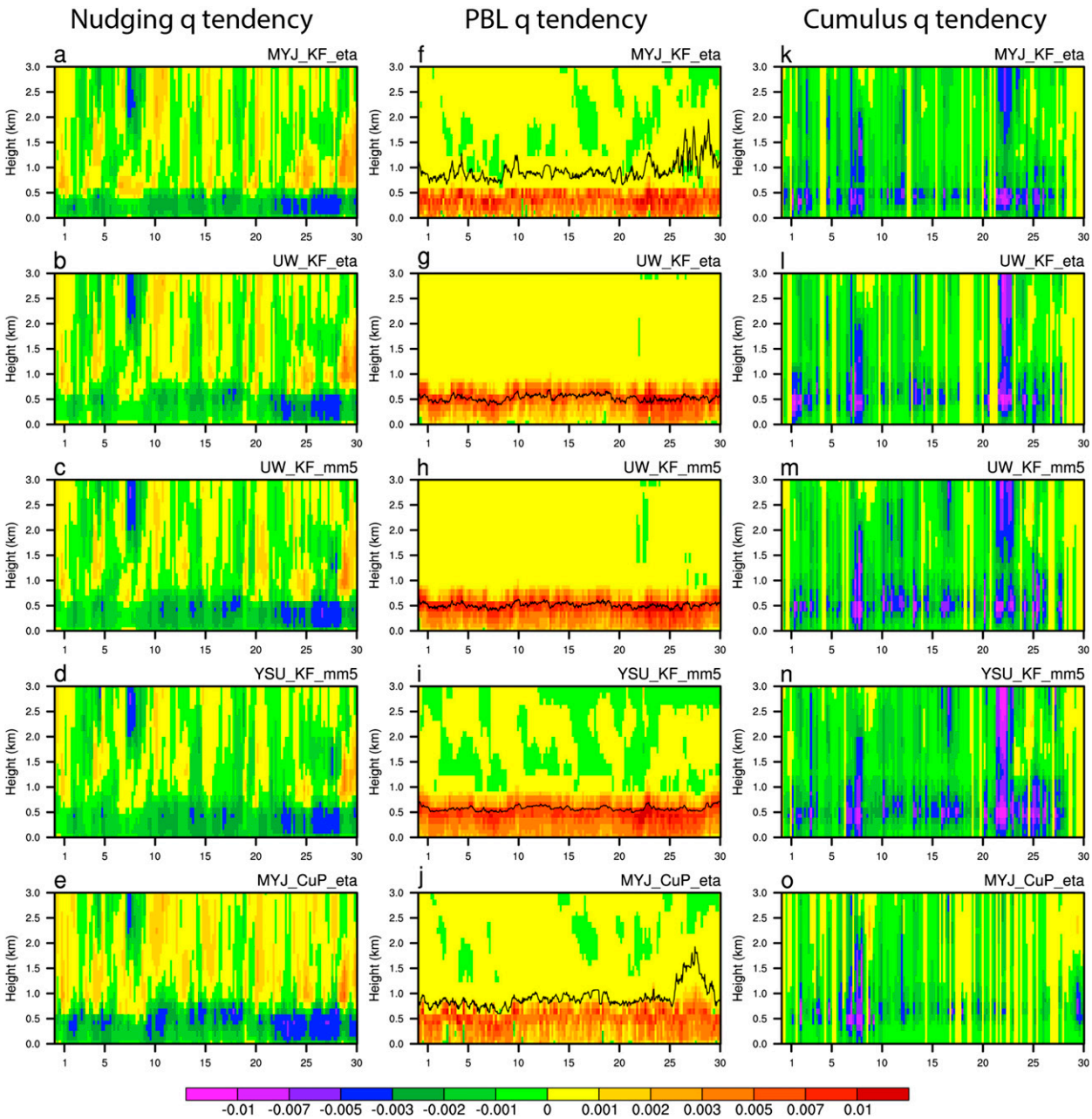

FIG. 8. Time–height variation of perturbation moisture-nudging terms and moisture tendency (kg m^{-2} day^{-1}) contributed by PBL and convection processes, respectively, averaged over the Maldives in November 2011 for simulations with different schemes. The black curves in the center are the simulated PBL heights based on the definition in different PBL schemes.

Diagnosing how the moisture-nudging process influences the model behavior helps identifying model biases and yields better understanding of the moistening process found in the free-running simulations. Figure 8 shows the time–height variation of perturbed moistening tendencies (the rate of moisture increase) associated with nudging to the observations, from the PBL scheme and from the cumulus parameterization, respectively, during November 2011. From Fig. 8 (center; PBL moisture tendency) we see the moistening from the PBL scheme takes place throughout the entire period in all three PBL schemes. While the moistening is almost uniformly distributed vertically and confined below the PBL top (~0.8 km) in the MYJ scheme, maximum moistening occurs near the top of the PBL in the UW and YSU schemes. With the same PBL scheme (UW), moistening

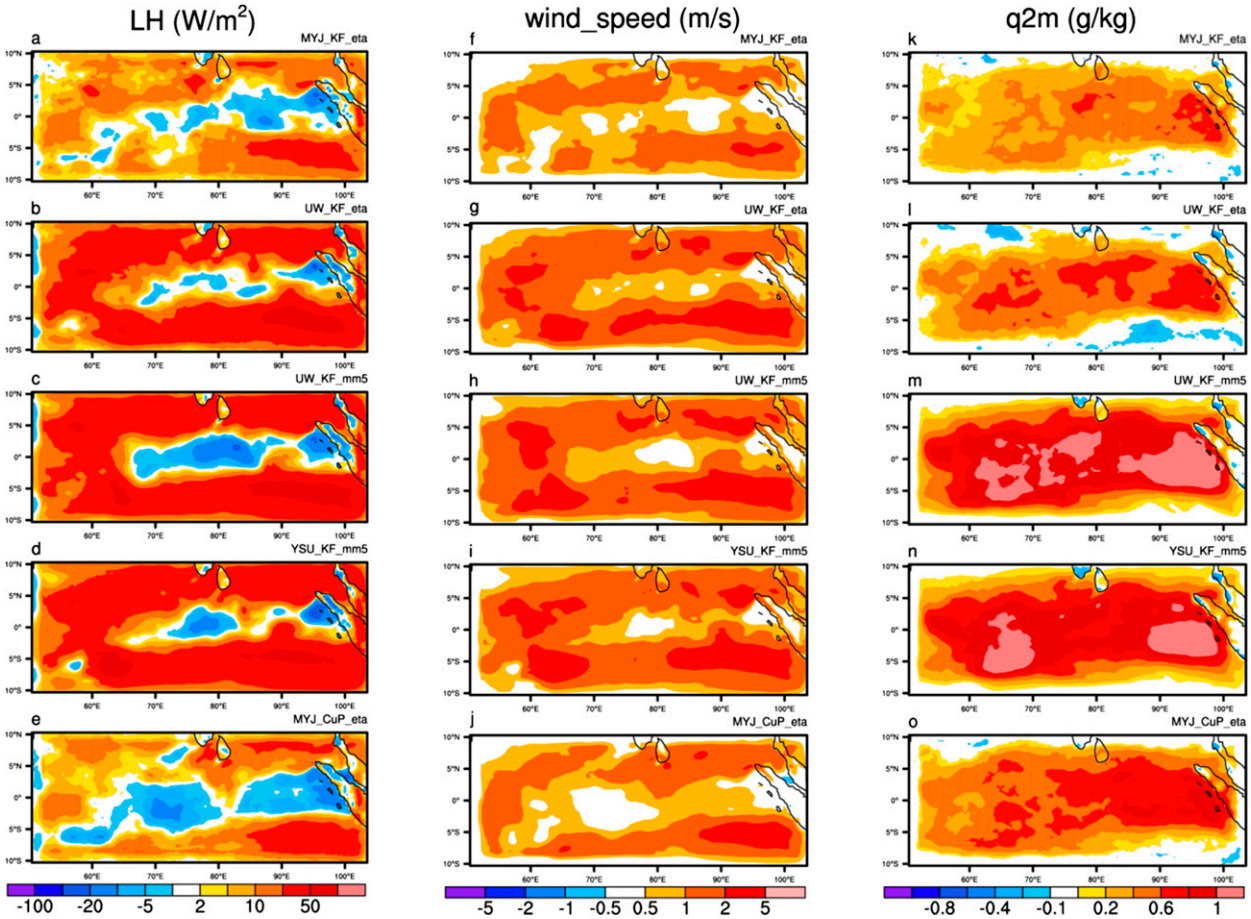

FIG. 9. Monthly mean difference of (left) LH flux, (center) wind speed, and (right) 2-m moisture between free and moisture-nudging experiments with different schemes as shown in Table 1.

is larger and extends deeper vertically when using the MM5 rather than in the Eta Model SL scheme because the MM5 scheme tends to bring more water vapor from the sea surface to the bottom of the boundary layer (Figs. 8g,h). The convective parameterization tends to dry the atmosphere from the surface to the top of the troposphere by transporting water vapor from the PBL into the free troposphere and converting water vapor to liquid water and precipitation, usually with maximum drying near the PBL top. In contrast to the PBL moistening throughout the entire period, Fig. 8 (right; convection moisture tendency) shows two convection drying episodes, corresponding to two deep convection events, one around 7 November and another around 22 November, in which a strong moisture drying extends from the surface to upper levels in the free troposphere. There are no significant differences in convective moisture tendency among the different PBL and SL schemes because moisture fields have already been nudged to reanalysis when a convection scheme is called in the model. However, it is surprising that the second episode of strong deep convection is missed in the simulations completed with the CuP shallow convection scheme, even when the nudging is applied, which is the main cause of the degradation of the precipitation in the MYJ–CuP–Eta nudging simulation. One likely explanation is that there are sufficient shallow clouds to vent the moisture from the PBL and limit the formation of the deep convection.

The nudging tendency term is proportional to the difference between the model-simulated moisture and that from reanalysis and works to reduce the deviation of the former from the latter. The moisture nudging artificially removes (adds) the overpredicted (underpredicted) water vapor in the free-running simulations so that the moisture distribution and profile after being adjusted can match that in the reanalysis data. The nudging moisture tendency could be used to quantify the model moisture bias in the free runs. From Fig. 8 (left) we can see that the nudged moisture tendency is negative within the PBL in all five simulations with

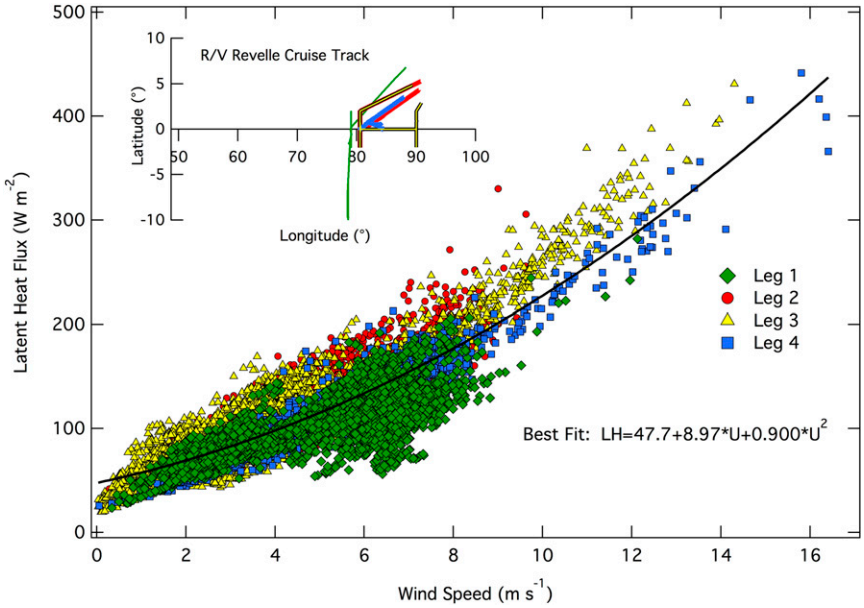

FIG. 10. Surface LH flux vs wind speed based on four R/V *Roger Revelle* cruise tracks marked in four colors in inset.

different parameterization schemes, with maximum values around 26–28 November, which indicates all PBL schemes significantly overpredict moisture within the PBL. Moisture nudging affects not only the availability and vertical distribution of water vapor but also the evolution of diabetic heating, consequently modifying the circulation, precipitation, and surface winds and fluxes. Figure 8 also shows the large negative moisture tendency due to the nudging process aloft in the free troposphere around 7 November, which removes water vapor and effectively reduces the wet precipitation bias (Fig. 4) for this event by enhancing the impact of dilution of the cumulus (Kain 2004).

The cause of the moisture bias in the free-running simulation can be better understood by examining differences in its results with the nudged simulations of surface LH flux, wind speed, and moisture (Fig. 9). Regardless of the model configuration, the nudging of the free-tropospheric moisture reduces LH fluxes over much of the domain and in particular the areas north and south of the main region of precipitation [red areas in Fig. 9 (left)]. This difference in LH fluxes is more or less reflected in the differences in surface wind speed as well (Fig. 9, center), both of which are overpredicted. The amount of near-surface moisture (Fig. 9, right) in the middle of the domain is also overpredicted in the free-running simulations. Overall, the nudging is found to reduce the precipitation, wind speed, and near-surface moisture. Results are less clear-cut for the LH flux, where there are large areas where the flux either increases or decreases in the simulations. Within WRF surface layer schemes, the surface LH flux is proportional to both the saturation deficit near the surface and the wind speed (Fairall et al. 1996). The fact that the nudging decreases surface LH flux over some areas even when it is increasing the saturation deficit (by decreasing the low-level moisture) suggests that the excess surface fluxes are related to the overestimate of surface wind speed. It is important to note that the wind speed across the center of the domain (within a few degrees of the equator) is largely unchanged between the two sets of the simulations. These areas are also associated with an increase in the surface LH fluxes in the nudged simulations [blue regions in Fig. 9 (left)]. In these areas, the overestimate of near-surface moisture in the free runs likely leads to the underprediction of surface LH flux in the center of the domain. These results also suggest that the free runs overestimate the low-level wind speed, and hence convergence near the equator, which when coupled with the excess near-surface moisture leads to the significant overprediction of the precipitation across most of the simulations domain. While these results are generally independent of model configuration, the impact of the nudging shown in Fig. 9 is smallest for the MYJ PBL parameterization as well as the Eta Model SL parameterization.

d. Diagnosis of surface evaporation

Surface evaporation or latent heat flux is mainly constrained by the wind speed, moisture exchange coefficient, and near-surface air humidity in this study

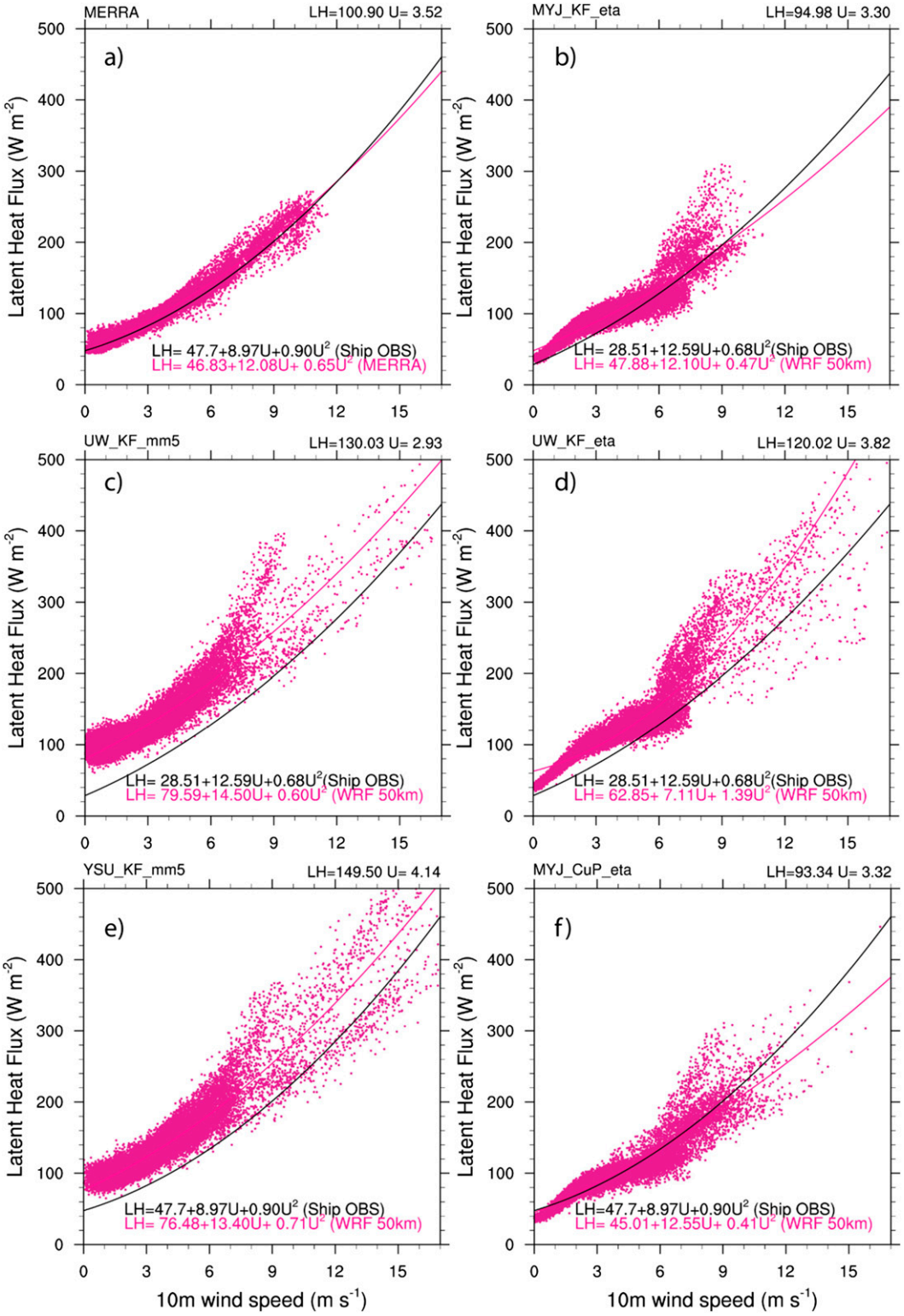

FIG. 11. Surface LH flux vs wind speed based on (a) MERRA data and (b)–(f) WRF simulations with different schemes. Fitting curves for observation (black) and each simulation (magenta) are also included.

TABLE 3. A summary of mean LH flux and 10-m wind speed from ship measurements and all simulations along the corresponding ship tracks.

Expt	Mean wind speed ($m\,s^{-1}$)	Skewness of wind speed	LH flux ($W\,m^{-2}$)
Ship obs	4.56	1.54	108.00
MERRA	3.52	1.12	100.90
MYJ–KF–Eta	3.30	0.76	94.98
UW–KF–Eta	3.82	1.92	120.02
UW–KF–MM5	2.93	1.55	130.03
YSU–KF–MM5	4.14	2.34	149.50
MYJ–CuP–Eta	3.32	1.06	93.34

because water is always abundant over the ocean surface and SST is prescribed from reanalysis data. To diagnose the source of bias in surface LH and its impact on the vertical water vapor transport in different schemes, we evaluated the simulated LH–wind speed relationships against the observations from near-surface meteorology measurements and surface LH fluxes estimates from the R/V *Roger Revelle* during the AMIE/DYNAMO field campaign. Figure 10 shows the relationship of LH flux versus wind speed along four R/V *Roger Revelle* cruise tracks (marked in four colors in the inset), and Fig. 11 shows the corresponding results from MERRA and our WRF simulations, in which fitted curves from observations are included for comparison.

Our results indicate that the biases of LH flux in our simulations are contributed by the bias of model-predicted wind speed and/or LH–wind speed relationship. Similar bias in a high-resolution WRF simulation (500-m grid spacing) in the same region is also reported by Feng et al. (2015), where enhanced LH flux is observed during the passage of precipitation-driven cold pools. When the same COARE version 3.0 bulk flux algorithm used for the R/V *Roger Revelle* data is applied to the model output, they found that the simulated surface LH flux is reduced by ~42% compared to the model output. These results suggest that 1) the model bias can be partly related to variations in the way that the fluxes were calculated and 2) model resolution is not the primary cause of the LH flux bias seen in our results. Here we provide a few highlights from the comparisons as summarized in Table 3 and Fig. 11.

1) The LH–wind speed relationship in MERRA agrees with in situ observations quite well. The averaged LH flux as shown in Table 3 is underestimated by approximately 8% in MERRA, contributed by the underestimated mean and skewness of the near-surface wind speed, probably due to the coarse spatial resolution in the reanalysis data.
2) With the same PBL (UW) and convection (KF) scheme (Figs. 11c,d), the MM5 SL scheme overpredicts the LH flux by more than 20% when compared against measurements, even though the mean wind speed is smaller than observed and the skewness of wind speed is comparable. This is mainly due to its oversimplified LH–wind speed relationship, resulting in nearly 10% larger LH flux than that in the Eta Model scheme. Weaker surface wind (i.e., larger friction) and larger LH flux in the MM5 scheme indicate stronger exchanges of momentum and moisture at the atmosphere–ocean interface.
3) With the same SL (Eta Model) and convection (KF) scheme (Figs. 11b,d), the UW PBL scheme generates larger LH flux than that in the MYJ PBL scheme by more than 20%, because of both larger wind speed and the steeper slope of the LH–wind speed relationship in the UW scheme. The differences in the LH–wind speed relationship can be traced, in part, to differences in the vertical mixing in the PBL. Figure 8 indicates that the UW scheme produces larger vertical mixing than the MYJ scheme, which favors transporting air from aloft with large downward momentum transport leading to larger surface wind speeds (Table 3 and Fig. 11). Meanwhile, low-level moisture is reduced because of stronger PBL mixing in the UW scheme (Figs. 5 and 6), indicating a larger ocean–air moisture contrast leading to enhanced evaporation. With the same MM5 SL scheme, the YSU PBL scheme, which shows the largest positive bias (~40%) in LH flux, generates a larger LH flux than that in UW PBL scheme by 15%, mainly because of the larger near-surface wind speed associated with stronger coupling between surface and air aloft in the nonlocal YSU scheme.
4) With the same PBL and SL scheme (Figs. 11b,f), the KF-CuP scheme simulates similar magnitude of wind speed and LH flux as the original KF scheme, which are slightly smaller than observations, resulting from the underestimate of wind speed and underestimated slope of LH flux versus wind speed.

In summary, the Eta Model surface layer scheme predicts more reasonable LH flux and better simulates the relationship between the LH and wind speed than the MM5 scheme, especially when it is coupled with the MYJ

scheme. When the Eta Model surface layer scheme is applied, the MYJ PBL scheme predicts a more reasonable LH–wind speed relationship than the UW scheme.

Shin and Hong (2011) and Xie et al. (2012) found that the Eta Model SL scheme could produce larger land–air exchange coefficients and stronger surface fluxes over continental or coastal regions when compared to the MM5 scheme, opposite to the results shown here for conditions over open ocean areas. This is because the formulas applied for the parameterization of SL processes are different over ocean and land in both schemes. Over the ocean, the surface roughness z_0 (m) is calculated based on u_* (m s^{-1}) in the MM5 scheme as follows:

$$z_0 = \frac{0.0185}{9.8} u_*^2 + 1.59 \times 10^{-5}. \quad (1)$$

In the Eta Model scheme, z_0 is calculated by the following:

$$z_0 = \max\left(\frac{0.018}{9.8} u_*^2, 1.59 \times 10^{-5}\right). \quad (2)$$

The value of u_* generally ranges from 0.1 to 0.2 m s^{-1} over ocean, which means z_0 is within the range from 1.8×10^{-5} to 7×10^{-5} m. As a result, the additional term (i.e., 1.59×10^{-5} m) applied in Eq. (1) can cause a large difference of z_0 even when u_* is about the same in the two schemes. Moreover, larger z_0 in the MM5 scheme will induce larger u_* that can in turn produce larger z_0 and thus stronger LH but weaker surface winds as shown in Fig. 11. This may be responsible for the overestimated LH at a given wind speed when using the MM5 scheme over the ocean. Under strong wind conditions, the additional term [i.e., 1.59×10^{-5} m in Eq. (1)] has a smaller impact on z_0 because of the larger value of u_*. In this case (e.g., wind speed >12 m s^{-1}), other factors such as the differences in the simulated u_* values and/or vertical moisture gradients between the two schemes play more important roles on the simulated LH, and the Eta Model scheme could produce larger values of LH than the MM5 scheme, similar to the results found over land (Shin and Hong 2011; Xie et al. 2012). As a result of this implementation, LH is more sensitive to wind speed when using the Eta Model scheme than using the MM5 scheme.

4. Conclusions

Based on observations collected during the 2011 AMIE/DYNAMO field campaign and model simulation results with different spatial resolutions and PBL, SL, and convection schemes, we reviewed the performance of various parameterizations that are available in WRF, version 3.4, for the representation of turbulent mixing. Comparison of the simulations with observations shows weaknesses of the model in capturing the characteristics of PBL processes, the initiation of convection, and intraseasonal variability of precipitation over the equatorial Indian Ocean, and we identify the source of biases by analyzing the dependence of these biases on PBL and surface layer schemes.

The results show that PBL and SL parameterizations have a surprisingly large impact on surface moisture flux, convective initiation, and precipitation over tropical oceans. All parameterizations tested tend to overpredict moisture in the PBL and free atmosphere and consequently produce larger moist static energy and surface precipitation. The updated shallow convection scheme KF-CuP tends to suppress the initiation and development of deep convection and consequently decrease precipitation over the domain. Moisture nudging tends to suppress the initiation of convection and reduces the overprediction of precipitation and provides additional insight in the behavior of the parameterizations. By analyzing the water vapor nudging tendency and tendencies from the PBL parameterization, we find that the vertical transport of water vapor is too active in all of the PBL schemes used in this study when applied over the ocean surface where moisture is abundant. This excess moisture and precipitation bias sustain each other through associated increased surface winds and LH fluxes. The Eta Model surface layer scheme predicts more reasonable LH fluxes and a more realistic LH–wind speed relationship than the MM5 scheme, especially when coupled with the MYJ scheme. By reviewing various parameterization schemes and their coupling in WRF, we identify the source of bias and weaknesses of the current PBL, SL, and SC schemes in capturing the characteristics of PBL and surface layer processes, the initiation of convection, and intraseasonal variability of precipitation, which could be used for improving the current implementation of the various parameterizations.

Simulations and analyses presented in this study were conducted over the ocean surface, where the moisture is always abundant, and it features relatively homogenous surface roughness, albedo, and surface water and energy fluxes. Hence, this study provides a good opportunity for better understanding the advantages and disadvantages of the PBL and convection schemes in WRF under "idealized" conditions. However, land–atmosphere–cloud interactions over land are much more complex because of the high spatiotemporal variability in surface water and energy fluxes as consequences of spatial heterogeneity in land cover, soil texture, topography, and human perturbations (e.g., irrigation) and thus warrant additional research to shed light on how to improve the

PBL and convection schemes under different climate and hydrologic regimes. In the near future, we will conduct similar studies over midlatitude and tropical continental regions to compare the model behavior with different parameterizations to investigate the transferability of the results from this study to other regions and to better understand the role of land surface heterogeneity in modulating PBL evolution and shallow convection as well as the regulation of soil moisture status on surface water and energy budgets and therefore land–atmosphere–cloud interactions, with the ultimate goal of improving land surface, boundary layer, and convection parameterizations in climate models.

Acknowledgments. We thank three referees for their careful review and constructive comments. This study was supported by the DOE Office of Science Biological and Environmental Research (BER) Atmospheric System Research (ASR) program (Grant 1830). We thank the DOE Atmospheric Radiation Measurement (ARM) programs for providing the ARM/CART data. The computations were performed using resources of the National Energy Research Scientific Computing Center (NERSC) at Lawrence Berkeley National Laboratory and PNNL Institutional Computing. PNNL is operated for the DOE by Battelle Memorial Institute under Contract DE-AC06-76RLO1830.

REFERENCES

Adler, R. F., and Coauthors, 2003: The version-2 Global Precipitation Climatology Project (GPCP) monthly precipitation analysis (1979–present). *J. Hydrometeor.*, **4**, 1147–1167, doi:10.1175/1525-7541(2003)004<1147:TVGPCP>2.0.CO;2.

Barker, H. W., R. Pincus, and J. J. Morcrette, 2003: The Monte-Carlo independent column approximation: Application within large-scale models. *Proc. GCSS/ARM Workshop on the Representation of Cloud Systems in Large-Scale Models*, Kananaskis, AB, Canada, GEWEX, 1–10.

Beljaars, A. C. M., 1995: The parametrization of surface fluxes in large-scale models under free convection. *Quart. J. Roy. Meteor. Soc.*, **121**, 255–270, doi:10.1002/qj.49712152203.

Berg, L. K., and R. B. Stull, 2004: Parameterization of joint frequency distributions of potential temperature and water vapor mixing ratio in the daytime convective boundary layer. *J. Atmos. Sci.*, **61**, 813–828, doi:10.1175/1520-0469(2004)061<0813:POJFDO>2.0.CO;2.

——, and ——, 2005: A simple parameterization coupling the convective daytime boundary layer and fair-weather cumuli. *J. Atmos. Sci.*, **62**, 1976–1988, doi:10.1175/JAS3437.1.

——, and S. Y. Zhong, 2005: Sensitivity of MM5-simulated boundary layer characteristics to turbulence parameterizations. *J. Appl. Meteor.*, **44**, 1467–1483, doi:10.1175/JAM2292.1.

——, W. I. Gustafson, E. I. Kassianov, and L. P. Deng, 2013: Evaluation of a modified scheme for shallow convection: Implementation of CuP and case studies. *Mon. Wea. Rev.*, **141**, 134–147, doi:10.1175/MWR-D-12-00136.1.

Betts, A. K., F. Chen, K. E. Mitchell, and Z. I. Janjić, 1997: Assessment of the land surface and boundary layer models in two operational versions of the NCEP Eta Model using FIFE data. *Mon. Wea. Rev.*, **125**, 2896–2916, doi:10.1175/1520-0493(1997)125<2896:AOTLSA>2.0.CO;2.

Bosilovich, M. G., 2008: NASA's Modern Era Retrospective Analysis for Research and Applications: Integrating Earth observations. EarthZine. [Available online at http://www.earthzine.org/2008/09/26/nasas-modern-era-retrospective-analysis/.]

Braun, S. A., and W. K. Tao, 2000: Sensitivity of high-resolution simulations of Hurricane Bob (1991) to planetary boundary layer parameterizations. *Mon. Wea. Rev.*, **128**, 3941–3961, doi:10.1175/1520-0493(2000)129<3941:SOHRSO>2.0.CO;2.

Bretherton, C. S., and S. Park, 2009: A new moist turbulence parameterization in the Community Atmosphere Model. *J. Climate*, **22**, 3422–3448, doi:10.1175/2008JCLI2556.1.

Bright, D. R., and S. L. Mullen, 2002: The sensitivity of the numerical simulation of the southwest monsoon boundary layer to the choice of PBL turbulence parameterization in MM5. *Wea. Forecasting*, **17**, 99–114, doi:10.1175/1520-0434(2002)017<0099:TSOTNS>2.0.CO;2.

Cha, D. H., D. K. Lee, and S. Y. Hong, 2008: Impact of boundary layer processes on seasonal simulation of the East Asian summer monsoon using a regional climate model. *Meteor. Atmos. Phys.*, **100**, 53–72, doi:10.1007/s00703-008-0295-6.

Chen, F., and J. Dudhia, 2001: Coupling an advanced land surface–hydrology model with the Penn State–NCAR MM5 modeling system. Part I: Model implementation and sensitivity. *Mon. Wea. Rev.*, **129**, 569–585, doi:10.1175/1520-0493(2001)129<0569:CAALSH>2.0.CO;2.

Cheng, A., and K. Xu, 2015: Improved low-cloud simulation from the Community Atmosphere Model with an advanced third-order turbulence closure. *J. Climate*, **28**, 5737–5762, doi:10.1175/JCLI-D-14-00776.1.

Cohen, A. E., S. M. Cavallo, M. C. Coniglio, and H. E. Brooks, 2015: A review of planetary boundary layer parameterization schemes and their sensitivity in simulating southeastern U.S. cold season severe weather environments. *Wea. Forecasting*, **30**, 591–612, doi:10.1175/WAF-D-14-00105.1.

Collins, W. D., and Coauthors, 2004: Description of the NCAR Community Atmosphere Model (CAM 3.0). NCAR Tech. Note NCAR/TN-464+STR, 214 pp. [Available online at http://www.cesm.ucar.edu/models/atm-cam/docs/description/description.pdf.]

de Szoeke, S. P., J. B. Edson, J. R. Marion, C. W. Fairall, and L. Bariteau, 2015: The MJO and air–sea interaction in TOGA COARE and DYNAMO. *J. Climate*, **28**, 597–622, doi:10.1175/JCLI-D-14-00477.1.

Ek, M. B., and Coauthors, 2003: Implementation of Noah land surface model advances in the National Centers for Environmental Prediction operational mesoscale Eta Model. *J. Geophys. Res.*, **108**, 8851, doi:10.1029/2002JD003296.

Emanuel, K. A., 2007: Environmental factors affecting tropical cyclone power dissipation. *J. Climate*, **20**, 5497–5509, doi:10.1175/2007JCLI1571.1.

Fairall, C. W., E. F. Bradley, D. P. Rogers, J. B. Edson, and G. S. Young, 1996: Bulk parameterization of air–sea fluxes for Tropical Ocean-Global Atmosphere Coupled-Ocean Atmospheric Response Experiment. *J. Geophys. Res.*, **101**, 3747–3764, doi:10.1029/95JC03205.

——, ——, J. E. Hare, A. A. Grachev, and J. B. Edson, 2003: Bulk parameterization of air–sea fluxes: Updates and verification

for the COARE algorithm. *J. Climate*, **16**, 571–591, doi:10.1175/1520-0442(2003)016<0571:BPOASF>2.0.CO;2.

Feng, Z., S. Hagos, A. K. Rowe, C. D. Burleyson, M. N. Martini, and S. P. de Szoeke, 2015: Mechanisms of convective cloud organization by cold pools over tropical warm ocean during the AMIE/DYNAMO field campaign. *J. Adv. Model. Earth Syst.*, **7**, 357–381, doi:10.1002/2014MS000384.

Golaz, J. C., V. E. Larson, and W. R. Cotton, 2002: A PDF-based model for boundary layer clouds. Part I: Method and model description. *J. Atmos. Sci.*, **59**, 3540–3551, doi:10.1175/1520-0469(2002)059<3540:APBMFB>2.0.CO;2.

Grenier, H., and C. S. Bretherton, 2001: A moist PBL parameterization for large-scale models and its application to subtropical cloud-topped marine boundary layers. *Mon. Wea. Rev.*, **129**, 357–377, doi:10.1175/1520-0493(2001)129<0357:AMPPFL>2.0.CO;2.

Guo, Z., and Coauthors, 2014: A sensitivity analysis of cloud properties to CLUBB parameters in the Single-Column Community Atmosphere Model (SCAM5). *J. Adv. Model. Earth Syst.*, **6**, 829–858, doi:10.1002/2014MS000315.

——, and Coauthors, 2015: Parametric behaviors of CLUBB in simulations of low clouds in the Community Atmosphere Model (CAM). *J. Adv. Model. Earth Syst.*, **7**, 1005–1025, doi:10.1002/2014MS000405.

Hagos, S., L. Y. R. Leung, and J. Dudhia, 2011: Thermodynamics of the Madden–Julian oscillation in a regional model with constrained moisture. *J. Atmos. Sci.*, **68**, 1974–1989, doi:10.1175/2011JAS3592.1.

——, Z. Feng, C. D. Burleyson, K. S. S. Lim, C. N. Long, D. Wu, and G. Thompson, 2014: Evaluation of convection-permitting model simulations of cloud populations associated with the Madden–Julian oscillation using data collected during the AMIE/DYNAMO field campaign. *J. Geophys. Res.*, **119**, 12 052–12 068, doi:10.1002/2014JD022143.

Hong, S. Y., and H. L. Pan, 1996: Nonlocal boundary layer vertical diffusion in a Medium-Range Forecast Model. *Mon. Wea. Rev.*, **124**, 2322–2339, doi:10.1175/1520-0493(1996)124<2322:NBLVDI>2.0.CO;2.

——, and J.-O. J. Lim, 2006: The WRF single-moment 6-class microphysics scheme (WSM6). *J. Korean Meteor. Soc.*, **42**, 129–151.

——, and S.-W. Kim, 2008: Stable boundary layer mixing in a vertical diffusion scheme. *Proc. Ninth Annual WRF User's Workshop*, Boulder, CO, National Center for Atmospheric Research, 3.3. [Available online at http://www2.mmm.ucar.edu/wrf/users/workshops/WS2008/abstracts/3-03.pdf.]

——, Y. Noh, and J. Dudhia, 2006: A new vertical diffusion package with an explicit treatment of entrainment processes. *Mon. Wea. Rev.*, **134**, 2318–2341, doi:10.1175/MWR3199.1.

Hu, X.-M., J. W. Nielsen-Gammon, and F. Zhang, 2010: Evaluation of three planetary boundary layer schemes in the WRF Model. *J. Appl. Meteor. Climatol.*, **49**, 1831–1844, doi:10.1175/2010JAMC2432.1.

——, D. C. Doughty, K. J. Sanchez, E. Joseph, and J. D. Fuentes, 2012: Ozone variability in the atmospheric boundary layer in Maryland and its implications for vertical transport model. *Atmos. Environ.*, **46**, 354–364, doi:10.1016/j.atmosenv.2011.09.054.

——, P. M. Klein, and M. Xue, 2013: Evaluation of the updated YSU planetary boundary layer scheme within WRF for wind resource and air quality assessments. *J. Geophys. Res. Atmos.*, **118**, 10 490–10 505, doi:10.1002/jgrd.50823.

Huang, H., A. Hall, and J. Teixeira, 2013: Evaluation of the WRF PBL parameterizations for marine boundary layer clouds: Cumulus and stratocumulus. *Mon. Wea. Rev.*, **141**, 2265–2271, doi:10.1175/MWR-D-12-00292.1.

Huffman, G. J., and Coauthors, 1997: The Global Precipitation Climatology Project (GPCP) combined precipitation dataset. *Bull. Amer. Meteor. Soc.*, **78**, 5–20, doi:10.1175/1520-0477(1997)078<0005:TGPCPG>2.0.CO;2.

Janjić, Z. I., 1990: The step-mountain coordinate: Physical package. *Mon. Wea. Rev.*, **118**, 1429–1443, doi:10.1175/1520-0493(1990)118<1429:TSMCPP>2.0.CO;2.

——, 1994: The step-mountain eta coordinate model: Further developments of the convection, viscous sublayer, and turbulence closure schemes. *Mon. Wea. Rev.*, **122**, 927–945, doi:10.1175/1520-0493(1994)122<0927:TSMECM>2.0.CO;2.

Jankov, I., W. A. Gallus, M. Segal, B. Shaw, and S. E. Koch, 2005: The impact of different WRF Model physical parameterizations and their interactions on warm season MCS rainfall. *Wea. Forecasting*, **20**, 1048–1060, doi:10.1175/WAF888.1.

Kain, J. S., 2004: The Kain–Fritsch convective parameterization: An update. *J. Appl. Meteor.*, **43**, 170–181, doi:10.1175/1520-0450(2004)043<0170:TKCPAU>2.0.CO;2.

——, and J. M. Fritsch, 1993: Convective parameterization for mesoscale models: The Kain–Fritsch scheme. *The Representation of Cumulus Convection in Numerical Models*, *Meteor. Monogr.*, No. 24, Amer. Meteor. Soc., 165–170.

Kummerow, C., W. Barnes, T. Kozu, J. Shiue, and J. Simpson, 1998: The Tropical Rainfall Measuring Mission (TRMM) sensor package. *J. Atmos. Oceanic Technol.*, **15**, 809–817, doi:10.1175/1520-0426(1998)015<0809:TTRMMT>2.0.CO;2.

Li, X. L., and Z. X. Pu, 2008: Sensitivity of numerical simulation of early rapid intensification of Hurricane Emily (2005) to cloud microphysical and planetary boundary layer parameterizations. *Mon. Wea. Rev.*, **136**, 4819–4838, doi:10.1175/2008MWR2366.1.

Mahfouf, J. F., E. Richard, P. Mascart, E. C. Nickerson, and R. Rosset, 1987: A comparative study of various parameterizations of the planetary boundary layer in a numerical mesoscale model. *J. Climate Appl. Meteor.*, **26**, 1671–1695, doi:10.1175/1520-0450(1987)026<1671:ACSOVP>2.0.CO;2.

Mellor, G. L., and T. Yamada, 1974: A hierarchy of turbulence closure models for planetary boundary layers. *J. Atmos. Sci.*, **31**, 1791–1806, doi:10.1175/1520-0469(1974)031<1791:AHOTCM>2.0.CO;2.

——, and ——, 1982: Development of a turbulence closure model for geophysical fluid problems. *Rev. Geophys.*, **20**, 851–875, doi:10.1029/RG020i004p00851.

Mohr, C. G., and R. L. Vaughan, 1979: An economical procedure for Cartesian interpolation and display of reflectivity factor data in three-dimensional space. *J. Appl. Meteor.*, **18**, 661–670, doi:10.1175/1520-0450(1979)018<0661:AEPFCI>2.0.CO;2.

Monin, A. S., and A. M. Obukhov, 1954: Basic laws of turbulent mixing in the ground layer of the atmosphere. *Tr. Geofiz. Inst., Akad. Nauk SSSR*, **151**, 163–187.

Pan, Z. T., S. G. Benjamin, J. M. Brown, and T. Smirnova, 1994: Comparative experiments with maps on different parameterization schemes for surface moisture flux and boundary-layer processes. *Mon. Wea. Rev.*, **122**, 449–470, doi:10.1175/1520-0493(1994)122<0449:CEWMOD>2.0.CO;2.

Pincus, R., H. W. Barker, and J. J. Morcrette, 2003: A fast, flexible, approximate technique for computing radiative transfer in inhomogeneous cloud fields. *J. Geophys. Res.*, **108**, 4376, doi:10.1029/2002JD003322.

Pleim, J. E., and J. S. Chang, 1992: A non-local closure model for vertical mixing in the convective boundary layer. *Atmos. Environ.*, **26**, 965–981, doi:10.1016/0960-1686(92)90028-J.

Qian, Y., M. Huang, B. Yang, and L. K. Berg, 2013: A modeling study of irrigation effects on surface fluxes and land–air–cloud interactions in the Southern Great Plains. *J. Hydrometeor.*, **14**, 700–721, doi:10.1175/JHM-D-12-0134.1.

Rowe, A. K., and R. A. Houze, 2014: Microphysical characteristics of MJO convection over the Indian Ocean during DYNAMO. *J. Geophys. Res. Atmos.*, **119**, 2543–2554, doi:10.1002/2013JD020799.

Ryzhkov, A. V., S. E. Giangrande, and T. J. Schuur, 2005: Rainfall estimation with a polarimetric prototype of WSR-88D. *J. Appl. Meteor.*, **44**, 502–515, doi:10.1175/JAM2213.1.

Shafran, P. C., N. L. Seaman, and G. A. Gayno, 2000: Evaluation of numerical predictions of boundary layer structure during the Lake Michigan Ozone Study. *J. Appl. Meteor.*, **39**, 412–426, doi:10.1175/1520-0450(2000)039<0412:EONPOB>2.0.CO;2.

Shin, H. H., and S. Y. Hong, 2011: Intercomparison of planetary boundary-layer parametrizations in the WRF Model for a single day from CASES-99. *Bound.-Layer Meteor.*, **139**, 261–281, doi:10.1007/s10546-010-9583-z.

Skamarock, W. C., and Coauthors, 2008: A description of the Advanced Research WRF version 3. NCAR Tech. Note NCAR/TN-475+STR, 113 pp. [Available online at http://www2.mmm.ucar.edu/wrf/users/docs/arw_v3.pdf.]

Sterk, H. A. M., G. J. Steeneveld, and A. A. M. Holtslag, 2013: The role of snow-surface coupling, radiation, and turbulent mixing in modeling a stable boundary layer over Arctic sea ice. *J. Geophys. Res. Atmos.*, **118**, 1199–1217, doi:10.1002/jgrd.50158.

Storm, B., J. Dudhia, S. Basu, A. Swift, and I. Giammanco, 2009: Evaluation of the Weather Research and Forecasting Model on forecasting low-level jets: Implications for wind energy. *Wind Energy*, **12**, 81–90, doi:10.1002/we.288.

Stull, R. B., 1984: Transilient turbulence theory. Part I: The concept of eddy-mixing across finite distances. *J. Atmos. Sci.*, **41**, 3351–3367, doi:10.1175/1520-0469(1984)041<3351:TTTPIT>2.0.CO;2.

Thompson, E. J., S. A. Rutledge, B. Dolan, and M. Thurai, 2015: Drop size distributions and radar observations of convective and stratiform rain over the equatorial Indian and west Pacific Oceans. *J. Atmos. Sci.*, **72**, 4091–4125, doi:10.1175/JAS-D-14-0206.1.

Troen, I., and L. Mahrt, 1986: A simple model of the atmospheric boundary layer sensitivity to surface evaporation. *Bound.-Layer Meteor.*, **37**, 129–148, doi:10.1007/BF00122760.

Troyan, D., 2012: Merged sounding value-added product. DOE-ARM Tech. Rep. DOE/SC-ARM/TR-087. [Available online at http://www.arm.gov/publications/tech-reports/doe-sc-arm-tr-087.pdf.]

Webster, P. J., A. M. Moore, J. P. Loschnigg, and R. R. Leben, 1999: Coupled ocean–atmosphere dynamics in the Indian Ocean during 1997–98. *Nature*, **401**, 356–360, doi:10.1038/43848.

Wyngaard, J. C., and R. A. Brost, 1984: Top-down and bottom-up diffusion of a scalar in the convective boundary layer. *J. Atmos. Sci.*, **41**, 102–112, doi:10.1175/1520-0469(1984)041<0102:TDABUD>2.0.CO;2.

Xie, B., J. C. H. Fung, A. Chan, and A. Lau, 2012: Evaluation of nonlocal and local planetary boundary layer schemes in the WRF Model. *J. Geophys. Res.*, **117**, D12103, doi:10.1029/2011JD017080.

Yang, Q., L. K. Berg, M. Pekour, J. D. Fast, R. K. Newsom, M. Stoelinga, and C. Finley, 2013: Evaluation of WRF-predicted near-hub-height winds and ramp events over a Pacific Northwest site with complex terrain. *J. Appl. Meteor. Climatol.*, **52**, 1753–1763, doi:10.1175/JAMC-D-12-0267.1.

Yoneyama, K., C. Zhang, and C. N. Long, 2013: Tracking pulses of the Madden–Julian oscillation. *Bull. Amer. Meteor. Soc.*, **94**, 1871–1891, doi:10.1175/BAMS-D-12-00157.1.

Zhang, D., and R. A. Anthes, 1982: A high-resolution model of the planetary boundary layer—Sensitivity tests and comparisons with SESAME-79 data. *J. Appl. Meteor.*, **21**, 1594–1609, doi:10.1175/1520-0450(1982)021<1594:AHRMOT>2.0.CO;2.

Zuluaga, M. D., and R. A. Houze, 2013: Evolution of the population of precipitating convective systems over the equatorial Indian Ocean in active phases of the Madden–Julian oscillation. *J. Atmos. Sci.*, **70**, 2713–2725, doi:10.1175/JAS-D-12-0311.1.